Supporting Information

Phase Identification and Strong Second Harmonic Generation in Pure ε-InSe and Its Alloys

Qiaoyan Hao,[†] Huan Yi,[†] Huimin Su,[‡] Bin Wei,[§] Zhuo Wang,[†] Zhezhu Lao,[∥] Yang Chai,[⊥]

Zhongchang Wang,[§] Chuanhong Jin,[∥] Junfeng Dai,[‡] Wenjing Zhang*,[†]

[†]International Collaborative Laboratory of 2D Materials for Optoelectronics Science and Technology, Shenzhen University, Shenzhen 518060, P. R. China

[‡]Department of Physics, Southern University of Science and Technology, Shenzhen 518055, P. R. China

[§]International Iberian Nanotechnology Laboratory, Av. Mestre Jose Veiga, P-4715330 Braga, Portugal

[∥]State Key Laboratory of Silicon Materials, School of Materials Science and Engineering, Zhejiang University, Hangzhou 310027, P. R. China

[⊥]Department of Applied Physics, Hong Kong Polytechnic University, Hong Kong 999077, P. R. China

EXPERIMENTAL SECTION

Synthesis of single crystals: Single crystal ε-InSe was synthesized by loading equimolar mixture of In (Macklin, 99.99%) and Se (Macklin, 99.999%) powder into a quartz tube, which was evacuated and sealed by oxy-hydrogen flame. Then the sealed tube was heated to 685 ℃ with 70 min and then heated to 700 ℃ within 5 min and kept at 700 ℃ for 3 days. After that, it was cooled to 500 ℃ within 2 days followed by naturally cooling. Both the Te- and S-alloyed samples were synthesized at the same experimental conditions by using stoichiometric amounts of raw materials.

XRD and scanning transmission electron microscopy (STEM) measurement: The as-synthesized crystals were ground into powder and collected X-ray Diffraction pattern using a Bruker D8 Advance X-ray diffractometer in a monochromatic Cu-Kα radiation of wavelength λ=1.5418 Å. The STEM images were acquired using a probe Cs-corrected transmission electron microscope (FEI Titan ChemiSTEM) with the high-angle annular dark-field (HAADF) and the bright field (BF) imaging techniques, and the energy dispersive X-ray spectroscopic (EDS) was used to characterize the elemental mapping of the as-prepared samples. The FEI Titan aberration-corrected ChemiSTEM operates at 200 kV with spot size of 8, Camera length 135 mm, condenser aperture of 70 μm, convergent angle 21 mrad. In addition, both the plane and cross-sectional selected area electron diffraction (SAED) patterns were taken in FEI Tecnai G^2 F20.

AFM, Raman and Photoluminescence Measurement: The few-layer and multilayer ε-InSe and its alloys were cleaved from as-synthesized crystals and adhered to the 300 nm SiO_2 coated Si by mechanical exfoliation method. The layer number of the flakes was determined by both optical image and atomic force microscope (AFM, Dimension ICON system, Bruker, USA) under ambient conditions. The Raman and PL spectra were taken by alpha300 system from WITec by using

excitation wavelength of 532 nm. The InGaAs CCD was employed to measure the PL spectra of the samples.

SHG measurement: The SHG measurement was carried out using a home-made microscope system. The samples were exfoliated and sealed in a home-made sample box with transparent cover in the glove box to remove the effects of air contamination. Femtosecond laser pulses at the wavelengths tunable from 800–1400 nm, with a repetition rate of 80 MHz and the pulse width of 150 fs, were used as the excitation source, which were focused on the sample using a 50X/NA 0.42 objective lens. The SHG signal was detected in a reflection geometry using a Horiba IHR320 spectrometer equipped with an ANDOR CCD camera.

Analysis of the three atomic columns as exhibited in Figure 2b and Figure 2f: The three atomic columns (X1, X2 and X3) can be figured in terms of atomic species and number. To make it clear, they are listed in Table S1 for different layer numbers ε-InSe. As reported in the reference, the atomic column intensity is contributed to a number of factors such as atomic number (Z), the specimen thickness, the crystal structure and the detector geometry.[1–3] First of all, the Z dependence of an atomic column is approximately proportional to $Z^{1.7}$. Besides, the individual atomic columns intensity correlates directly with the number of atoms in each column.[4] For thin STEM specimen, the Z dependence of image intensity (I) can be approximated by $I \sim Z^{\alpha}$, where α is in the range of 1.6–1.9.[5] Since indium has a higher Z value (Z_{In}=49) compared with selenium (Z_{Se}=34), the strongest atomic columns of X1 site must be occupied by the superposition of both In and Se atoms, while the stronger atomic columns of X3 site are expected to be occupied by the single In atoms and the weakest X2 site occupied by the single Se atoms. Afterwards, STEM simulation based on the structure of ε-InSe was performed in order to understand the contribution of specimen thickness to the observed Z-contrast along the [001] zone axis. Complex and gradual

variations in *Z*-contrast of *N* (two–100) layer appear in the Figure S2, which can be accounted for the dispersion of In and Se atoms in the aforementioned three atomic columns. By careful comparison between experimental and simulated atomic column intensities, the experimental result agrees with that of *N* (four–ten) layer ε-InSe (Figure 2f).

Table S1. The atomic species and number of the three atomic columns mentioned in the text for ε-InSe with different layer numbers. Note that due to the noncentrosymmetric structure of ε-InSe, the relative location of the three sites alters if the crystal lattice is rotated by 180 ° along the [001] zone axis. However, according to the STEM simulation results of few-layer (two–ten layers) ε-InSe, the X3 site shows brighter contrast than the X2 site, so it should be occupied by heavier In atoms rather than Se atoms.

Layer number	X1	X2	X3
1	2In		2Se
2	2In+2Se	2Se	2In
3	2In+4Se	2Se	4In
4	4In+4Se	4Se	4In
5	4In+6Se	4Se	6In
6	6In+6Se	6Se	6In
N (odd number)	(*N*-1)In+(*N*+1)Se	(*N*-1)Se	(*N*+1)In
N (even number)	(*N*)In+(*N*)Se	(*N*)Se	(*N*)In

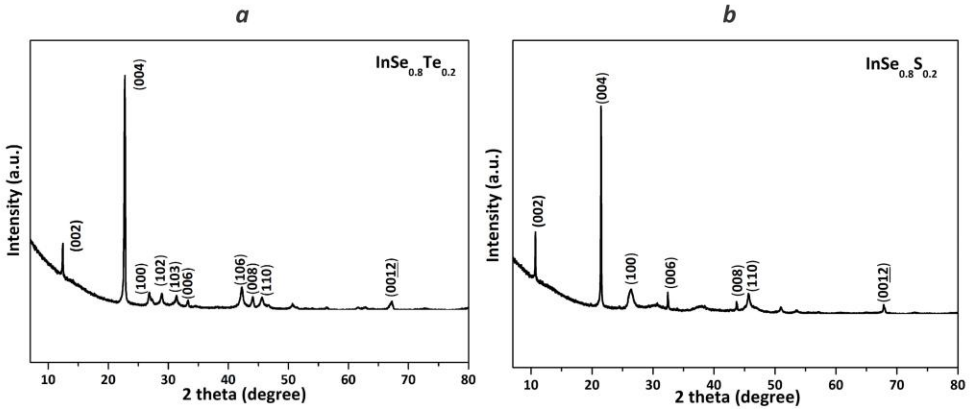

Figure S1. XRD patterns of alloyed samples: (a) $InSe_{0.8}Te_{0.2}$ and (b) $InSe_{0.8}S_{0.2}$.

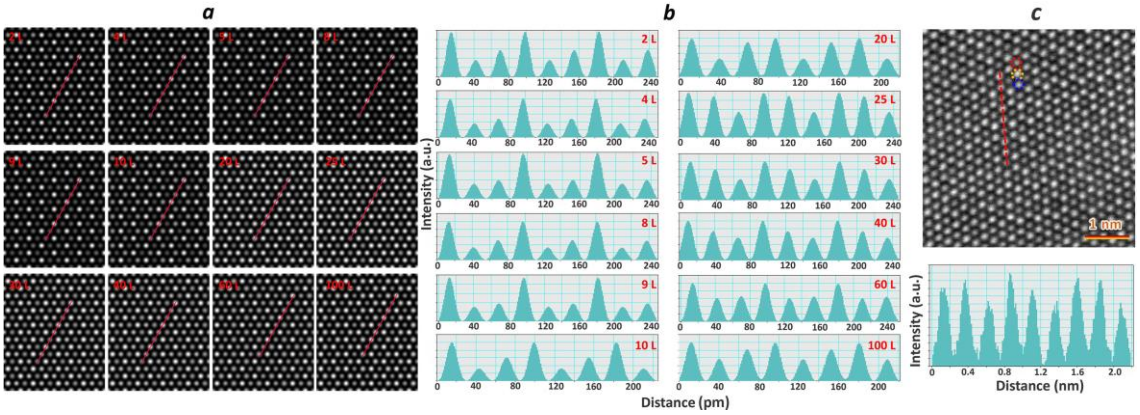

Figure S2. (a) Simulation results of HAADF-STEM along the [001] zone axis of *N* layer ε-InSe (*N*=two-100). (b) Intensity profiles corresponding to the red solid lines in (a). (c) HAADF-STEM image taken from thicker ε-InSe nanosheet and the experimental intensity profile corresponding to the red dashed line. The experiment result agrees with the simulation result of ~25 layers ε-InSe.

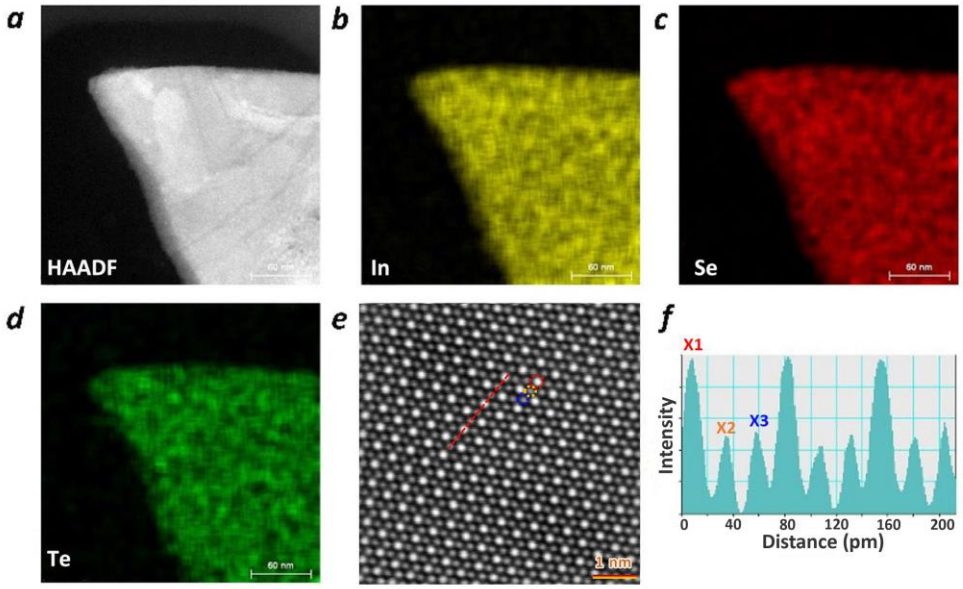

Figure S3. Z-Contrast imaging and intensity analysis of $InSe_{0.8}Te_{0.2}$. (a) High-angle annular dark-field image of $InSe_{0.8}Te_{0.2}$ nanosheet. (b-d) EDS mapping of the region (a) with a scale bar of 60 nm. (e) HAADF-STEM image taken from the marginal area in (a). (f) Experimental intensity profile corresponding to the red dashed line marked in (e).

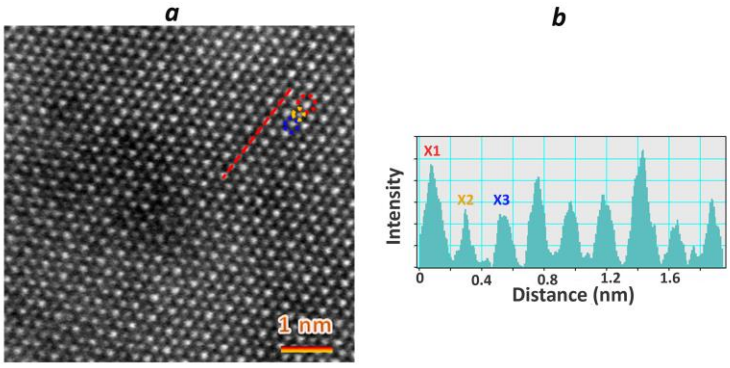

Figure S4. Z-Contrast imaging and intensity analysis of $InSe_{0.8}S_{0.2}$. (a) HAADF-STEM image taken from $InSe_{0.8}S_{0.2}$ nanosheet. (b) Experimental intensity profile corresponding to the red dashed line marked in (a).

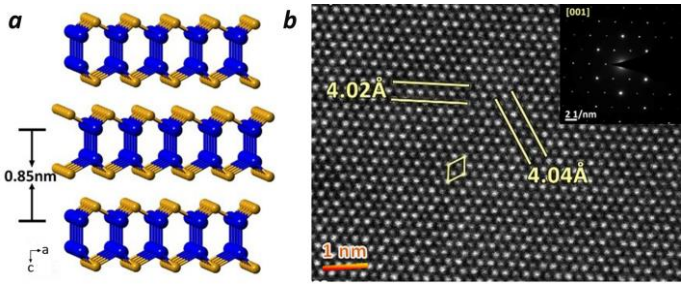

Figure S5. (a) Calculated crystal structure of ε-InSe with the c-axis vertical. Gold and blue spheres represent Se and In atoms respectively. (b) HAADF-STEM image projected along [001] zone axis, the insert is its corresponding SAED pattern.

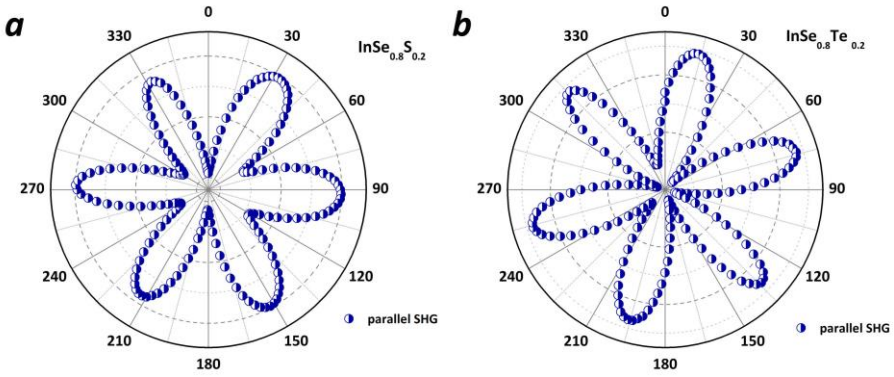

Figure S6. Polarization-resolved SHG intensities of $InSe_{0.8}S_{0.2}$ (a) and $InSe_{0.8}Te_{0.2}$ (b) as a function of the excitation laser polarization against the crystalline lattice direction.

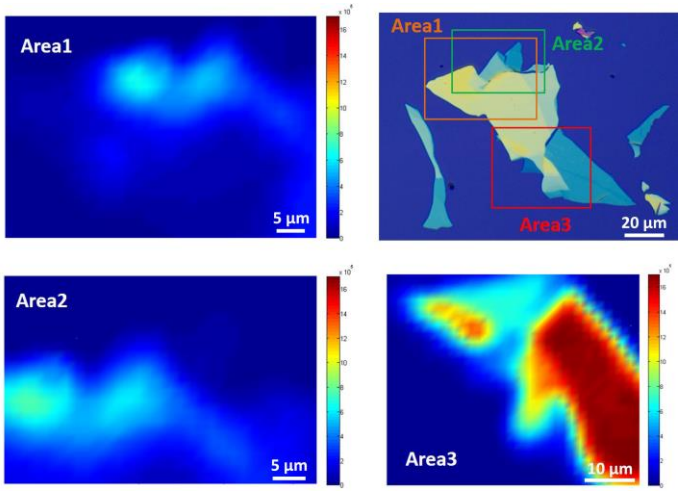

Figure S7. Optical image and SHG mapping on ε-InSe flakes under excitation of λ_{ex} = 1000 nm.

The second-order nonlinear susceptibility $\chi^{(2)}$ could be calculated by[6]:

$$I_{2\omega} = \left[\chi^{(2)}\right]^2 I_{\omega}^2 8\epsilon_0 c^3 \cdot \frac{1}{n_{2\omega} n_{\omega}^2} \cdot \frac{\omega^2 d^2}{8\epsilon_0 c^3} \quad \text{(S1)}$$

Where ϵ_0 is the vacuum dielectric constant; c is the light speed in vacuum; ω is the frequency of the excitation laser; d is the thickness of the layered crystals; $n_{2\omega}$ and n_{ω} are refractive indexes of bulk crystals under SHG and excitation laser frequency, respectively.[7–11] Note that $n_{2\omega}$ of InSe under excitation laser of 800 and 900 nm is estimated to be approximately equal to that of GaSe because of the similarity of the reported refractive indexes between InSe and GaSe crystals at different excitation laser. $I_{2\omega}$ and I_{ω} are the peak intensities of excitation laser and SHG signal, respectively. They are related with the peak power ($P_{2\omega}$ and P_{ω}) by:

$$I_{2\omega} = \frac{2P_{2\omega}}{\epsilon_0 c\, \pi R_{2\omega}^2} \quad \text{(S2)}$$

$$I_{\omega} = \frac{2P_{\omega}}{\epsilon_0 c\, \pi R_{\omega}^2} \quad \text{(S3)}$$

Where $P_{2\omega}$ and P_{ω} are the peak power of the second harmonic wave and the pulsed laser, respectively, which can be calculated according to the reference.[12] $R_{2\omega}$ and R_{ω} are the radius of the second harmonic wave and the pump laser, respectively. As many parameters should be considered in calculating the value of $\chi^{(2)}$, such as frequency and duration of the excitation laser, the shape and size of the focused fundamental laser spot on the samples, and the relation between the measured spectral counts and the actual SHG power, the parameter of optical elements in the experimental setup, the results in Table S2 may have one order of magnitude estimation. However, the

comparison of $\chi^{(2)}$ among different samples is meaningful as they were measured under controlled conditions.

Table S2. Comparison of $\chi^{(2)}$ among multilayer (~20 nm) ε-InSe, multilayer (~20 nm) GaSe and monolayer WS_2 at excitation wavelength of 800 and 900 nm, respectively.

	InSe	GaSe	WS_2	InSe	GaSe
$\chi^{(2)}$ (10^{-11} m V^{-1})	1.3	1.1	0.2	4.9	1.6
Excitation λ (nm)	800	800	800	900	900

References

(1) Wang, Z. W.; Li, Z. Y.; Park, S. J.; Abdela, A.; Tang, D.; Palmer, R. E. Quantitative Z-Contrast Imaging in the Scanning Transmission Electron Microscope with Size-Selected Clusters. *Phys. Rev. B: Condens. Matter Mater. Phys.* **2011**, *84*, 073408.

(2) Pennycook, S. J.; Boatner, L. A. Chemically Sensitive Structure-Imaging with a Scanning Transmission Electron Microscope. *Nature* **1988**, *336*, 565–567.

(3) Muller, D. A. Structure and Bonding at the Atomic Scale by Scanning Transmission Electron Microscopy. *Nat. Mater.* **2009**, *8*, 263–270.

(4) Li, Z. Y.; Young, N. P. ; Di Vece, M.; Palomba, S.; Palmer, R. E.; Bleloch, A. L.; Curley, B. C.; Johnston, R. L.; Jiang, J.; Yuan, J. Three-Dimensional Atomic-Scale Structure of Size-Selected Gold Nanoclusters. *Nature* **2008**, *451*, 46–48.

(5) Hartel, P.; Rose, H.; Dinges, C. Conditions and Reasons for Incoherent Imaging in STEM. *Ultramicroscopy* **1996**, *63*, 93–114.

(6) Zhou, X.; Cheng, J. X.; Zhou, Y. B.; Cao, T.; Hong, H.; Liao, Z. M.; Wu, S. W.; Peng, H. L.; Liu, K. H.; Yu, D. P. Strong Second-Harmonic Generation in Atomic Layered GaSe. *J. Am. Chem.*

Soc. **2015**, *137*, 7994–7997.

(7) Piccioli, N.; Toullec, R. L.; Mejatty, M.; Balkanski, M. Refractive Index of GaSe Between 0.45 μm and 330 μm. *Appl. Optics* **1977**, *16*, 1236–1238.

(8) Liu, H. L.; Shen, C. C.; Su, S. H.; Hsu, C. L.; Li, M. Y.; Li, L. J. Optical Properties of Monolayer Transition Metal Dichalcogenides Probed by Spectroscopic Ellipsometry. *Appl. Phys. Lett.* **2014**, *105*, 201905.

(9) Kato, K.; Tanno, F.; Umemura, N. Sellmeier and Thermo-Optic Dispersion Formulas for GaSe (Revisited). *Appl. Optics* **2013**, *52*, 2325–2328.

(10) Celustka, B.; Persin, A.; Bidjin, D. Refractive Index of Thin Monocrystal Films of InSe. *J. Appl. Phys.* **1970**, *41*, 813–814.

(11) Bringuier, E.; Bourdon, A.; Piccioli, N. Chevy, A. Optical Second-Harmonic Generation in Lossy Media: Application to GaSe and InSe. *Phys. Rev. B: Condens. Matter Mater. Phys.* **1994**, *49*, 16971–16982.

(12) Wang, Z.; Dong, Z.; Zhu, H.; Jin, L.; Chiu, M. H.; Li, L. J.; Xu, Q.; Eda, G.; Maier, S. A.; Wee, A. T. S.; Qiu, C.; Yang, J. K. W. Selectively Plasmon-Enhanced Second-Harmonic Generation from Monolayer Tungsten Diselenide on Flexible Substrates. *ACS Nano* **2018**, *12*, 1859–1867.